Special Issues –International Symposium on Polymer Crystallization 2007–

Temperature Dependence of Crystal Growth Rate for α and β Forms of Isotactic Polypropylene

By Kayo NAKAMURA,[1] Satoko SHIMIZU,[1] Susume UMEMOTO,[1] Annette THIERRY,[2] Bernard LOTZ,[2] and Norimasa OKUI[1,*]

The crystal growth rate of the α_1, α_2 and β forms of isotactic polypropylene (iPP) and their morphological changes were studied in a wide range of crystallization temperatures. The temperature dependence of the crystal growth rate of the α_1 form showed a bell-shaped curve with the maximum growth rate (G_{max}) at 70 °C. The crystal growth rate of the β form induced by calcium pimelate also showed a bell-shaped curve with G_{max} at 79 °C. Two crossover points on the growth rate curve from the α_1 form to the β form or vice versa were observed at 90 °C and 133 °C, respectively. Tear-drop shaped spherulites were observed at temperatures between the two crossover points. Electron diffraction patterns showed the high ordered structure of the α_2 form for thin films crystallized at 140 °C. The α_2 fraction became detectable in X-ray diffraction pattern for temperatures above 110 °C. The α_2 fraction increased with crystallization temperature and saturated to 100% at about 140 °C. In the temperature region from 110 °C to 140 °C, several crystal growth rates were found at the same crystallization temperature. The growth rate variations could be associated with the co-crystallization of the α_1 and α_2 forms. Above 140 °C, the growth rate variations disappeared, since the fraction of the α_2 reached to 100%. The extrapolated G_{max} of the α_2 showed at 72 °C.
KEY WORDS: Isotactic Polypropylene / α-Form / β-Form / Crystal Growth Rate / Crossover /

Isotactic polypropylene (iPP) is one of the most widely used commercial polymeric materials and has been extensively investigated for it academic and industrial interest. iPP displays different structural polymorphism, such as α form (monoclinic), β form (trigonal), γ form (orthorhombic) and smectic form, which all consist of 3_1 helical conformations with a 0.65 nm chain axis periodicity. The α form is the most common crystal structure, which is produced by crystallization from the melt or solution.[1–5] The β form can be obtained from temperature gradient crystallization,[6] crystallization under molecular orientation[7] or can be induced by selective β-nucleating agent.[8–10] The crystal structure of the α form was first determined by Natta and Corradini.[11] Mencik[12] and Hikosaka and Seto[13] showed that the α structure has two limiting modifications named α_1 and α_2 forms. Extensive works on these crystalline forms have been also reported.[14–16] The α_1 form space group (C2/c) is the limit-disordered structure and the α_2 form (P2$_1$/c) is the limit-ordered structure. They are characterized by either regular alternation of the up and down orientations of the methyl group along the chain (α_2) or random orientation. A transition from the α_1 form to the α_2 form is observed by annealing at a higher temperature.[17–22] The crystal structure of the β form has been analyzed by Meille *et al.*[23] and refined by D. L. Dorset *et al.*[9]

Many studies about the crystallization behavior and morphology of iPP have been reported. When iPP was crystallized from the melt in a wide temperature range, Keith and Padden found four distinct spherulites, classified on the basis of their birefringence as I (positive), II (negative), III (highly negative), and IV (negative and banded).[1] There is an additional spherulite type with mixed positive and negative birefringence.[2] Types of I, II and mixed crystallize in the α-modification and types of III and IV are characteristic of the β crystal form. Optical properties of the α phase spherulites are strongly dependent on the extent of lamellar branching.[3–5] The lamellar branching is observed only for the α and γ crystalline modifications, not for its β modification. Positive spherulites are formed when highly branched α-form lamellae are produced. The lamellar branching is due to a homo-epitaxy on the lateral (010) face of the α-form crystallites.[5] It is interesting to note that I and II type spherulites show almost the same crystal growth rates. Coexistence of the α and β forms is often observed at the same crystallization temperature, with the β form being usually a minority constituent in the absence of β-nucleating agent. Temperature dependence of these crystal growth rates shows a crossover point (or bifurcation growth) at about 140 °C.[18,20,21] Below 140 °C, the growth rate of the β form is faster than α form, but their rates are reversed above 140 °C. On the other hand, when iPP is crystallized at a relatively low temperature, the growth rate of α form will be faster again than that of β form. In fact, the crossover point from α to β has been found at about 105 °C during stepwise crystallization[19,22] on the basis of morphological changes. It has been difficult to demonstrate this low crossover point by the

[1]Department of Organic and Polymeric Materials, International Polymer Research Center, Tokyo Institute of Technology, 2-12-1, Ookayama, Meguro-ku Tokyo, Japan
[2]Institut Charles Sadron (CNRS-ULP), 6 Rue Boussingault, 67083 Strasbourg, France
*To whom correspondence should be addressed (Tel/Fax: +81-3-5734-2469, E-mail: okui.n.aa@m.titech.ac.jp).

crystal growth measurements, because of the very high growth rates in this temperature range.

For many polymers, the temperature dependence of the spherulite growth rate shows a distinct discontinuity. For iPP, a visible discontinuity, or more exactly an inflexion point of the growth rate curve is observed around 140 °C.[24] The temperature at the discontinuity and the growth rate are strongly dependent on molecular weight[25] and isotacticity[26] of iPP. The discontinuity in the growth rate has been interpreted as a II–III regime transition.[24–28] However, the crystal growth rate is influenced by several factors, such as crystal phase transition, change in radial growth direction, tacticity and molecular weight. Among these factors, a change of the crystal phase has a major impact on the temperature dependence of the crystal growth rate.[29–31] For example, poly(lactic acid:PLLA)[30] and poly(butylene adipate:PBAd)[31] have two (or more) crystal modifications. Jumps of the growth rate are observed for both PLLA and PBAd. They have been associated with a transition between crystal modifications.

Transferring these observations to isotactic polypropylene, one may wonder whether the (small) change of growth rates from α_1 to α_2 is associated. Whereas such a possibility has not been explored, it is attractive especially since structural and growth kinetics data are accessible. The two crystal modifications display indeed characteristic differences in their X-ray diffraction patterns. To ease measurements of growth rates, we use an iPP sample of relatively low tacticity. The crystal growth rates are thus significantly reduced, especially at low temperatures, which also allow rapid transfer from the melt to these low temperatures. The crystal growth rates of the α and β forms were measured independently in a wide range of crystallization temperatures. This range covers in particular the maximum growth rate (G_{max}) that has been reported to be characteristic of polymer crystallization.[32,33] The crossover points between the α and β forms are determined by their crystal growth rates at high and low temperatures. Also, we discuss the relationship between the crystal growth rate characteristics and the crystal form transition for α_1 and α_2 forms as a function of temperature.

EXPERIMENTAL

Isotactic polypropylene (iPP) is commercially available (Aldrich Chemical Company Inc.). We used two different molecular weight samples; sample-A ($M_n = 67,000$, $M_w/M_n = 3.2$, pentad isotacticity = 88.1%) and sample-B ($M_n = 97,000$, $M_w/M_n = 3.8$, pentad isotacticity = 88.7). Calcium pimelate was used as a nucleation agent for the β form of iPP. For transmission electron microscopy (TEM) observations, thin films were prepared by casting dilute solutions of iPP in *p*-xylene on cleaved mica sheets. The thin films were melted at 180 °C for 5 min and crystallized isothermally at 125 °C and 145 °C in a Linkam LK-600 hot stage under nitrogen atmosphere. Subsequently, the thin films were coated by carbon, floated on water, and mounted on copper grids. Electron diffraction patterns were obtained with a Philips CM12

operated at 120 kV, and equipped with a rotation tilt stage (tilt angle ±60°). Molecular modeling and calculation of the diffraction patterns were performed with the Cerius[2] package (Accelrys Inc. San Diego). For growth rate measurements, the samples were sandwiched between cover glasses mounted in a Linkam LK-300 hot stage under a polarized optical microscopy (POM: OLYMPUS BH-2) equipped with a sensitive tint plate. The samples were melted on a hot stage at 220 °C for 5 min, then cooled down to a given crystallization temperature (T_c), and subsequently crystallized at various T_c. The fastest cooling rate of the LK-300 stage was used. Nominally, it is 5000 K/min, but the actual cooling rate is lower, in view of the low thermal conductivity of polymeric materials. The crystal growth rates (spherulite radius as a function of time) for the α and β forms were measured independently under the POM for sample free of or seeded with calcium pimelate (0.07 wt %). For wide-angle X-ray diffraction (WAXD) measurements, the samples were sandwiched between glass slides with a thickness of 0.5 mm, melted at 220 °C for 5 min, and subsequently crystallized isothermally at various T_c under Mettler FP80-82 heating stage. The crystallized samples were removed from the glass slides, and WAXD patterns were recorded with a RINT-2000 system (Rigaku Corp., Japan) with Cu-Kα radiation operating at 40 kV and 40 mA. The system was equipped with a pin-hole collimator and a graphite monochromator in line, and the X-ray intensity was measured in a symmetrical-transmission (θ-2θ) mode using a scintillation counter. The peaks were analyzed using standard curve fitting programs. The crystal melting temperature was recorded on a Shimazu TA60 (DSC) at a heating rate of 10 °C/min. The equilibrium melting temperature was determined by the Hoffman-Weeks extrapolation method.[34]

RESULTS AND DISCUSSION

Crystal Growth Rates of α and β forms

Figure 1 shows the crystallization temperature dependence of spherulite growth rates of α and β forms. Both crystal growth rates are measured in a wide temperature range (50–155 °C) and show bell-shaped curves with their maximum growth rates (G_{max}). (Sample-A showed a similar temperature dependence of the crystal growth rate.) The α and β forms of
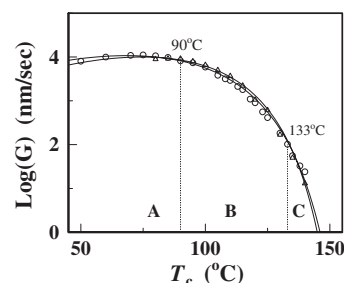

Figure 1. Crystallization temperature dependence of spherulite growth rate for sample-B. ($\triangle$): β form in the presence of calcium pimelate (0.07 wt %). ($\bigcirc$): α form in the absent of nucleation agent. Solid curves indicate results for the best fitting using eq 1.

iPP can be easily distinguished under POM because the β form spherulites are highly birefringent, in sharp contrast with the α form spherulites. It must be pointed out that the growth rates of the α form display some scatter at any given crystallization temperature when the temperature exceeds $110\,°C$. The origin of this dispersion will be discussed in a later section. Here, the lowest crystal growth rate is considered as the growth rate of the α form, since the continuity in the growth rate curve is observed in a wide range of temperature throughout $110\,°C$.

Crystal growth rate data are often analyzed by a classical crystallization theory proposed by Lauritzen and Hoffman.[35] The growth rate is given by eq 1,

$$G = G_o \exp[-\Delta E/RT - \Delta F/RT] \qquad (1)$$

where G_o is a constant without temperature dependence but that strongly depends on the molecular weight[32] and ΔE is the activation energy for the molecular transport process. ΔF is the work required to form a secondary nucleus of critical size and is commonly expressed as $\Delta F = K T_m°/\Delta T$. K is a secondary nucleation parameter expressed as $n\sigma_e\sigma_s/\Delta H_m$, where n is a mode of nucleation, ΔH_m is the heat of fusion, σ_e and σ_s are the end- and lateral-surface free energies, respectively. ΔT is the degree of super-cooling $(T_m°\text{-}T)$, where $T_m°$ is the equilibrium melting temperature and T is crystallization temperature. R is the gas constant. The ΔE and ΔF terms have opposite temperature dependence; thereby bringing about a maximum (G_{max}) in the growth rate. The solid curves in Figure 1 correspond to a best fitting based on eq 1. Here, the equilibrium melting temperatures observed by Hoffman-Weeks plots were $174.2\,°C$ for the α form and $169.4\,°C$ for the β form. These equilibrium melting temperatures of relatively low tacticity iPP used in this work are approximately consistent with the reference data for the α form[26] and the β form.[20] The maximum growth rates for the α and β forms are observed at $70\,°C$ and at $79\,°C$.

The ratio of these growth rates (G_β/G_α) varies with crystallization temperature, with the maximum at about $118\,°C$ as seen in Figure 2. It had been reported early on that the β phase grow from *ca.* 20 to 70% faster than the α phase $(G_\alpha < G_\beta)$.[1] Intersection of crystal growth rate from β to α form (or bifurcation growth at higher temperature: $G_\alpha > G_\beta$) has been observed at about $140\,°C$.[18,20] On the other hand, in the temperature range below about $105\,°C$, it has been predicted that G_α becomes faster again than G_β (bifurcation
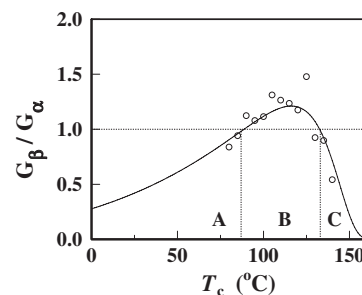
Figure 2. Ratio of spherulite growth rate of the α and β forms (G_α/G_β) for sample-B.

at low temperature) on the basis of a morphological change of spherulite.[19,22] These results indicate that two growth rate intersections appear on temperature dependence of spherulite growth rate curves for α and β forms. In fact, two crossover points are observed clearly by the present work as seen in Figure 1, defining three temperature regions, below $90\,°C$ (lower crossover), between $90\,°C$ to $133\,°C$ and above $133\,°C$ (higher crossover) marked as A, B and C. These crossover points coincide with reference data,[17–22] except for their actual temperatures. The present crossover temperatures are $7–15\,°C$ lower than those from references. These differences could be associated with a difference in isotacticity. Low isotacticity gives rise to lower melting and lower crossover temperatures. It has been pointed out that morphological behavior of the β-nucleated copolymers (propylene/α-olefin) is similar to that of the homopolymer, but the rate of crystallization and the characteristic temperatures decrease with increasing co-mono-mer unit.[36]

In region A, the growth rate of the α form is faster than that of the β form. However, the nucleation rate of the β form can be significantly increased when using beta phase specific nucleating agents. Figure 3(A) shows the optical micrograph of spherulite crystallized at $90\,°C$. The center of the spherulite is of the β form and the outer ring of the spherulite (surrounding the β form) is of the α form. The negative spherulite of the β form appear first and then the α form is crystallized later at the external side of the β spherulite. The β form central region probably formed first on cooling, and transition to the α form took place when the temperature became lower than the β-α crossover point. In region B in the presence of the β nucleation agent, two different spherulites are formed with different
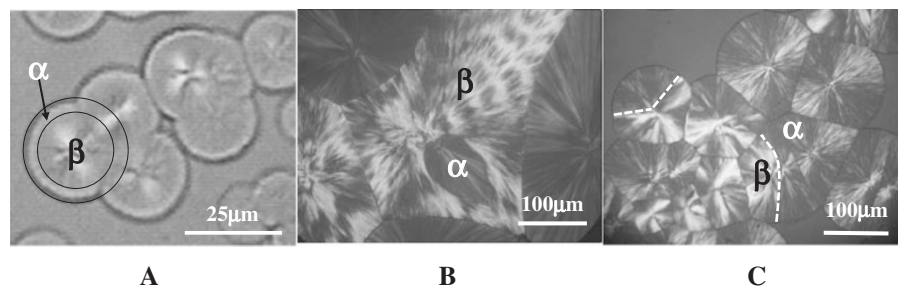
Figure 3. Optical micrograph of spherulites for sample-B crystallized at $90\,°C$ (A), $130\,°C$ (B) and $140\,°C$ (C) in the presence of calcium pimelate ($0.07\,wt\%$).
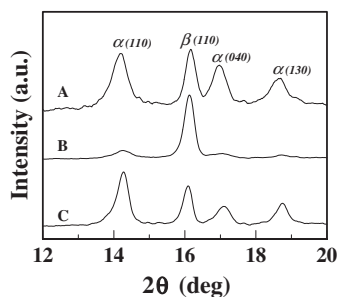
Figure 4. X-Ray diffraction patterns for sample-B crystallized at 90 °C (A), 130 °C (B), 140 °C (C) in the presence of calcium pimelate (0.07 wt %).

growth rates, showing a tear-drop-shaped α phase spherulite embedded in a β form spherulite. Also the presence of the two forms is confirmed by melting experiments; the melting of the tear part (α form) takes place at higher temperatures than that of the outer parts (β form). This tear shaped morphology is often observed in i-PP[6,37,38] and other polymers.[39,40] In region C, the β form spherulite is enveloped by the α form one, because of the faster growth rate of the latter α form. The β to α transition is observed by optical microscopy.[6,18,20] Figure 4 shows X-ray diffraction patterns obtained in the three regions for sample-B. In region A, the α and β forms coexist (Figure 4(A)). In region B, the β form increases with increasing in T_c (Figure 4(B)). The amount of the β form should decrease with temperature above 118 °C, since the ratio (G_β/G_α) decreases above 118 °C as seen in Figure 2. The relative amount of the α and β forms depend, however, also on the efficiency of the β nucleating agent. A similar impact allows for the observation of some β form in region C, where $G_\alpha > G_\beta$ (Figure 4(C)).

Crystal Growth Rates of α_1 and α_2 forms

Figure 5 shows optical micrographs of α phase spherulites crystallized at 120 °C, 130 °C and 150 °C, showing positive, mixed and negative spherulites, respectively. Spherulites of α form iPP are usually classified in three types;[1,2] positive (type-I), mixed and negative spherulites (type-II) with increasing crystallization temperature. The birefringence of iPP α spher-

ulites depends on the relative proportions of radial and tangential lamellae and on the orientation of the parent and daughter lamellae relative to the light path.[3–5] The positive spherulite is associated with the highly branching structure of α-form phase of lamellae, which are due to homo-epitaxy on the lateral face of (010) in the α-form crystallite.[5] The lamellar branching is observed only for the α crystalline modification, not for its β modification (also, the γ phase branches on the α phase, but not on itself). It is positive for high density of branching, but may become mixed to negative with decreasing branching density.

There are two limiting modifications in the α form, named α_1 and α_2 forms. The α_1 form (C2/c) is the limit-disordered structure and the α_2 form (P2$_1$/c) is the limit-ordered structure. They are characterized by regularity of the up and down positions of the methyl group along the chain. Irreversible transition from the α_1 form to the α_2 form is observed by annealing at high temperature.[12–16,41–44] The helical arrangement (right and left handed helix) in the α_2 form is the same as that in the α_1 form. For the up or down arrangement (the projected direction of methyl group onto the c-axis), the α_1 form is the limit-disordered structure while the α_2 form is the limit-ordered structure. There are several papers for α form about X-ray diffraction.[11–16] It is reported that the most drastic differences between the X-ray fiber diffraction patterns of the α_1 and α_2 forms are observed along the 1st layer line.[15] The α_1 and α_2 forms cannot be differentiated on the basis of their {hk0} reflections only. The positions of methyl group for up and down chains are maintained and only the positions of main chain atoms are slightly different in chain axis projection. However, the {hkl} reflections depend on the regularity of up or down arrangement and the more ordered structure (of lower symmetry) displays additional reflections. Therefore, it is possible to distinguish the α_1 and α_2 forms based on the {hkl} reflections electron diffraction pattern. Figure 6 shows TEM (a) and ED (b) for the cast thin film crystallized at 125 °C for sample-A. It displays the diffraction spots associated with the α_1 form, in good agreement with the calculated pattern as shown in Figure 6(c). When the sample is crystallized at 145 °C, lath-like lamellae are observed as seen in Figure 7(a). The ED pattern shown in Figure 7(b), indicates that the long
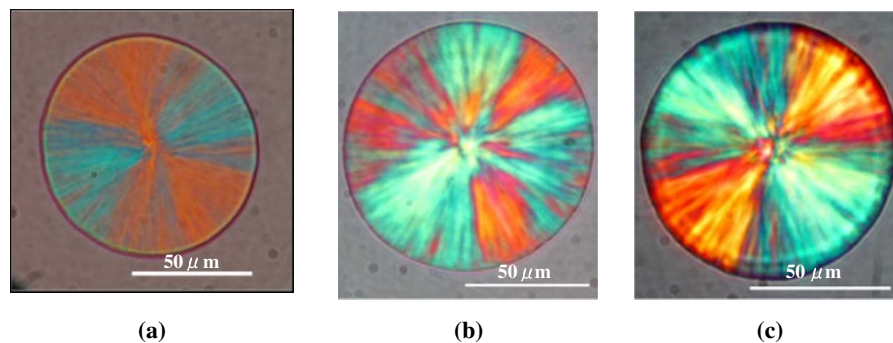

(a) (b) (c)

Figure 5. Optical micrograph of spherulites of sample-B crystallized at (a) 120 °C (positive spherulite), (b) 130 °C (mixed spherulite) and (c) 150 °C (negative spherulite).
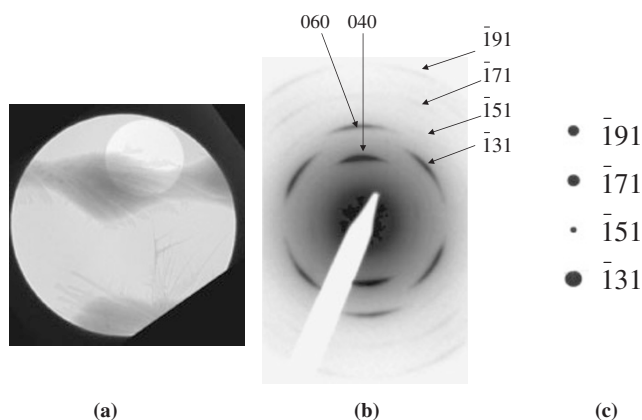
(a)   **(b)**   **(c)**

Figure 6. Electron micrograph (a) and electron diffraction pattern (b) of the cast thin film of sample-A crystallized at 125 °C (α_1 form) and calculated ($\bar{1}$k1) reflections (c).
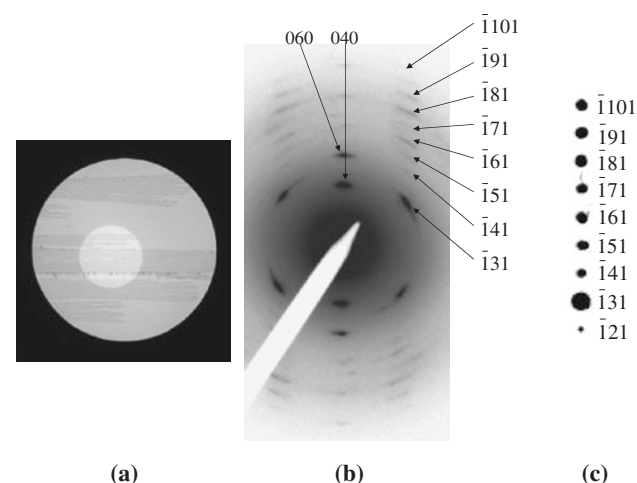

(a)   **(b)**   **(c)**

Figure 7. Electron micrograph (a) and electron diffraction pattern (b) of the cast thin film for sample-A crystallized at 145 °C (α_2 form) and calculated ($\bar{1}$k1) reflections (c).

axis of the lath crystal is the a-axis and the direction perpendicular to the lath is the b-axis. The ED pattern indicates the α_2 form, since many ($\bar{1}$k1) reflections are seen in Figure 7(b). These reflections can be brought in diffraction conditions by tilting the crystal by 50° around the b axis in the tilting stage of the electron microscope. The first layer line reflections of the α form are very telling when considering the structural order (or disorder) discussed above. Additional reflections are seen in Figure 7(b) as compared to Figure 6(b). The observed diffraction pattern is in good agreement with the calculated pattern of the α_2 form shown in Figure 7(c). However, the ED method cannot evaluate quantitatively the amount of the α_2 form in the sample.

Figure 8 shows a typical WAXD pattern recorded from the sample crystallized at 140 °C and the peak separation. The inset in figure shows the profile expanded in the range of $2\theta = 28$–35°. WAXD pattern of the α_1 form is the same as the α_2 for (hkl) reflections where h + k = even. On the other hand when h + k = odd, the (hkl) reflections are systematically absent
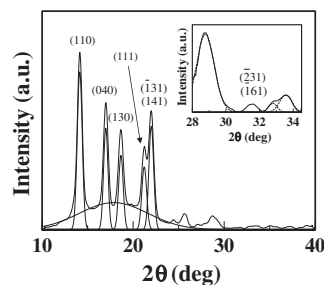

Figure 8. Typical WAXD pattern and decomposition in different diffraction peak for sample-B crystallized at 140 °C. The inset shows the expanded profile in the 2θ range 28–34.5°.
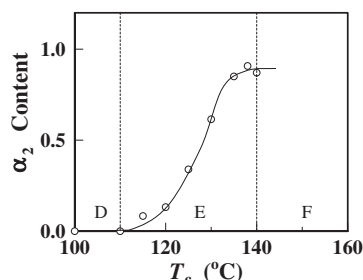

Figure 9. Variation of the α_2 form fraction for sample-B crystallized in the range 100–145 °C, dividing three regions D (below 110 °C), E (from 110 °C to 140 °C) and F (above 140 °C).

owing to the extinction rule in the α_1 form. The α_2 form thus can be detected easily by its most typical and strongest reflections ($\bar{2}$31) and ($\bar{1}$61) in the vicinity of $2\theta = 31.6°$, where reflections of the α_1 form can not be detected. According to the reference method,[13] the α_2 fractions were estimated based on the intensity of ($\bar{2}$31) and ($\bar{1}$61) which was normalized by the intensity of (110) reflection. The calculated α_2 fractions for sample-B are plotted as a function of crystallization temperature as shown in Figure 9, dividing three regions marked as D, E and F (similar α_2 fractions were observed for sample-A). The α_2 form begins to be detectable in X-ray diffraction patterns above 110 °C (region E). Its fraction increases with crystallization temperature and saturates at about 140 °C (region F) (note however that the 100% mark indicated in Figure 9 should not be taken literally, but indicates merely a saturation point. The exact percentage is unknown). It is interesting to note that the α_2 fraction can be evaluated by NMR,[45] which also indicates an increase of the α_2 fraction with crystallization temperature. It has been already reported in many papers that the α_2 fraction increases with crystallization temperature[46] and/or annealing temperature.[41–44] On annealing, the α_2 form fraction rapidly increases with time and saturates within 10 min.[44] This indicates that the structural ordering (transformation from α_1 to α_2) is completed early on in the annealing process. Also, the lattice parameters for a-axis and c-axis of the α_1 form increase slightly on heating. On the other hand, the thermal expansion of the b-axis increases significantly up to 155 °C but decreases on transformation to the α_2 form.[44] This variation provides direct evidence for the transformation from
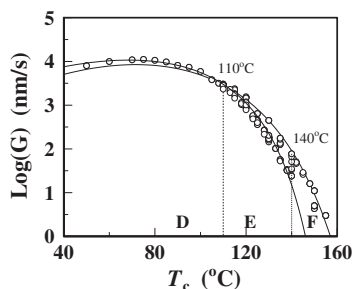
Figure 10. Temperature dependence of crystal growth rate for sample-B. Various growth rates are found in region E, but not in regions of D and F. Solid curves indicate results for the best fitting using eq 1.

Figure 11. Logarithm of the difference between the highest and lowest growth rates in region E as a function of the α_2 fraction.

the disordered (α_1) to ordered (α_2) structures. Here, a molecular process of growth of the α_2 crystal can be performed in the matrix α_1 crystallites. That is, the transformation from the α_1 to α_2 would imply that neighboring molecules exchange their positions.

When iPP was crystallized at higher temperatures, DSC curves showed double melting peaks. These double melting peaks have been reported previously.[41,42,46] The lower melting peak can be attributed to the α_1 form and the higher peak to the α_2 form. Based on these two melting peaks (so-called Hoffman Weeks plots), two equilibrium melting temperatures were extrapolated; one was 174.2 °C, which coincides with the equilibrium melting temperature of the α_1 form reported elsewhere.[26] The other was 208 °C, which could be the equilibrium melting temperature of the α_2 form. Note that the equilibrium melting temperature of the α_2 phase has not been reported previously. Figure 10 shows the temperature dependence of the crystal growth rate for the α form in a wide range of temperatures for sample-B (a similar temperature dependence of the crystal growth rate was observed for sample-A). It can be divided into three regions (D, E and F), as in Figure 9. Below 110 °C (region D), reproducible crystal growth rates are observed. Several growth rates (or a dispersion of the rates) are often observed at the same crystallization temperature above 110 °C (region E). The growth rate scatter may reflect some experimental errors or factors—or they may have a more fundamental origin. However, the above X-ray results suggest that these results might be attributable to co-crystallization of the α_1 and α_2 forms. Above 140 °C (region F), when the α_2 fraction saturates, reproducible single growth rates are observed again. It is interesting to note that in region E the data dispersion follows closely the increment of the α_2 fraction. At this stage, it must be pointed out that the type of spherulite is positive (type I) in region D, mixed in region E and negative (type II) in region F as seen in Figure 5. As the α_2 fraction increases, the growth rates become quite scattered (several growth rates at the same T_c). Here, it might be assumed that these growth rates are related to the mixture of the α_1 and α_2 forms in the same spherulites. These forms co-crystallize side-by-side statistically in the same spherulites. That is, limit ordered and limit disordered structures locate randomly in the same spherulites. The ratio of these limit
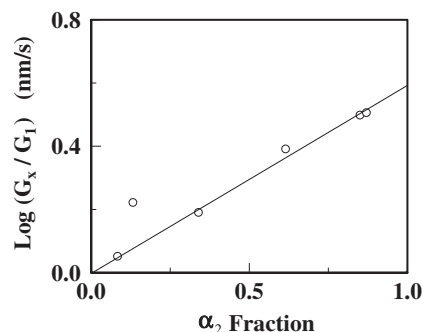
structures will change as a function of T_c. In fact, the index of the up and down ordering of the chains increases with annealing or crystallization temperature.[41,46] The limit ordered structure is preferable to generate at higher temperatures.

Such co-crystallization of the α_1 and α_2 forms in the same spherulites will give rise to change in the spherulite growth rate as a function of the relative amount of these forms. Here, it could be thought that the α_1 and α_2 forms are statistically dispersed in the same spherulite. The spherulite growth rate (G_x) can be assumed to be a function of the fraction (X) of the other component (like polymer blends) as the following equation.

$$dG_x/dX = -kX \tag{2}$$

Integrate the above equation and set-up the boundary conditions ($G_x = G_1$ when $X = 0$ (pure α_1 form), $G_x = G_2$ when $X = 1$ (pure α_2 form)), then we can get the following equation.

$$Ln(G_x/G_1) = XLn(G_2/G_1) \tag{3}$$

This equation indicates that the logarithm of spherulite growth (G_x) changes linearly with the fraction of the α_2 form at a constant T_c. Figure 11 shows plots of the growth rate difference between the lowest and highest growth rates at the same T_c as a function of the α_2 fraction. There are several growth rates, which might be depending on the amount of α_2 forms in the spherulite. In other words, there are α_1-form rich spherulites and α_2-form rich spherulites, when the sample is crystallized above 110 °C. However, when the fraction of α_2 saturates the growth rate variation disappears.

Based on the above results, the lowest and highest growth rates in Figure 10 can be attributed to the α_1 and α_2 forms, respectively. Thus two curves are obtained from a best fitting based on eq 1 with equilibrium temperatures of 174.2 °C for α_1 and 208 °C for α_2. The maximum growth rates for the α_1 and α_2 forms can be estimated at 70 °C and 72 °C, respectively. It looks like a puzzle why the growth rate of α_2 (more ordered structure) is faster than that of α_1. According to a crystallization kinetic theory given by eq 1, the growth rate must be considered at a constant super-cooling rather than at a constant T_c. In fact, Figure 12 shows that the growth rate of α_2 is slower than that of α_1 at the constant super-cooling, since the equilibrium melting temperature of α_2 is higher than that of
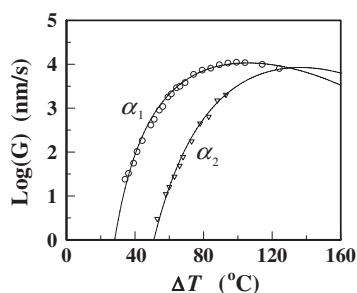
Figure 12. Super-cooling dependence of natural logarithm of crystal growth rate of the lowest (α_1) (○) and the highest (α_2) (▽) rates as seen in Figure 10. Solid curves indicate results for the best fitting using eq 1. $T_m° = 174.2$ °C for the α_1 form and $T_m° = 208$ °C for the α_2 from are used.

α_1. There is another quiz why a low tacticity iPP shows such growth rate variation, since those variations in a high taxticity iPP have not been reported. There are several defects in iPP, such as atactic, syndiotactic and head-to-head (or tail-to tail) sequences. These defects may be possible to generate a change in helical arrangement (left and right handed helix) or chain direction (up and down). The head-to-head defect can produce the chain direction from the up to down or vice versa. However, the head-to-head defect can be neglected in iPP prepared by Zieglar-Natta catalyst. (Sample used in this work is produced by Zieglar-Natta catalyst.) The conformational defect can provide the reversal of helical hand along the chain.[47,48] The reversal activity enhances the nucleation of α_2 crystal depositing their molecules on the crystal growth front. Such nucleation process can give rise to several crystal growth rates, depending on the α_2 fraction coexisting of α_1 crystal on the growing crystal surface.

CONCLUSION

The crystal growth rate of the α_1, α_2 and β forms and their morphological changes were studied in a wide range of crystallization temperatures. The temperature dependence of the crystal growth rate of the α_1 form showed a bell-shaped curve with the maximum growth rate (G_{max}) at 70 °C. The crystal growth rate of the β form induced by calcium pimelate also showed a bell-shaped curve with G_{max} at 79 °C. Two crossover points on the growth rate curve from the α_1 form to the β form or vice versa were observed at 90 °C and 133 °C, respectively. The tear-drop spherulite shape of α form was observed between the two crossover points. When the sample was crystallized above 110 °C, the α_2 form began to be detectable in X-ray diffraction pattern. Electron diffraction patterns showed the high ordered structure of the α_2 form for the thin film crystallized at 140 °C. The α_2 fraction was estimated from X-ray diffraction pattern as a function of crystallization temperature. The α_2 fraction increased with temperature and saturated at about 140 °C. In crystallization temperature ranges from 110 °C to 140 °C, several crystal growth rates (growth rate dispersion) were found at the same crystallization temperature. Above 140 °C, the growth rate

variations disappeared, since the fraction of the α_2 reached to 100%. The growth rate dispersion could be associated with co-crystallization of the α_1 and α_2 forms, whereas the pure α_1 and α_2 forms were observed below 110 °C and above 140 °C, respectively. The extrapolated G_{max} of the α_2 showed at 72 °C.

REFERENCES

1. F. J. Padden and H. D. Keith, *J. Appl. Phys.*, **30**, 1479 (1959).
2. D. R. Norton and A. Keller, *Polymer*, **26**, 704 (1985).
3. F. L. Binsbergen and B. G. M. De Lange, *Polymer*, **9**, 23 (1968).
4. F. Khoury, *J. Res. Natl. Bur. Stand.*, **70A**, 29 (1966).
5. B. Lotz and J. C. Wittman, *J. Polym. Sci., Part B: Polym. Phys.*, **24**, 1541 (1986).
6. A. J. Lovinger, J. O. Chua, and C. C. Gryte, *J. Polym. Sci., Polym. Phys. Ed.*, **15**, 641 (1977).
7. J. Varga and J. Karger-Kocsis, *J. Polym. Sci., Part B: Polym. Phys.*, **34**, 657 (1996).
8. J. Varga, *J. Macromol. Sci.*, **B41**, 1121 (2002).
9. D. L. Dorset, M. P. McCourt, S. Kopp, M. Schumacher, T. Okihara, and B. Lotz, *Polymer*, **39**, 6331 (1998).
10. T. Kawai, R. Iijima, Y. Yamamoto, and T. Kimura, *Polymer*, **43**, 7301 (2002).
11. G. Natta and P. Corradini, *Nuovo Cimento Suppl.*, **15**, 40 (1960).
12. Z. Mencik, *J. Macromol. Sci.*, **B6**, 101 (1972).
13. M. Hikosaka and T. Seto, *Polym. J.*, **5**, 111 (1973).
14. A. Immirzi and P. Iannelli, *Macromolecules*, **21**, 768 (1988).
15. F. Auriemma, O. R. de Ballesteros, C. De Rosa, and P. Corradini, *Macromolecules*, **33**, 8764 (2000).
16. M. Hirose, T. Yamamoto, and M. Naiki, *Comp. Theor. Polym. Sci.*, **10**, 345 (2000).
17. J. Varga and F. Toth, *Makromol. Chem. Macromol. Symp.*, **5**, 213 (1986).
18. J. Varga, Y. Fujiwara, and A. Ille, *Periodica Polytech. Chem. Eng.*, **34**, 255 (1990).
19. B. Lotz, B. Fillon, A. Thierry, and J. C. Wittmann, *Polym. Bull.*, **25**, 101 (1991).
20. G. Y. Shi, X. D. Zhang, and Z. X. Qiu, *Makromol. Chem.*, **193**, 583 (1992).
21. J. Varga, *J. Mater. Sci.*, **27**, 2557 (1992).
22. B. Lotz, *Polymer*, **39**, 4561 (1998).
23. S. V. Meille, D. R. Ferro, S. Bruckner, A. J. Lovinger, and F. J. Padden, *Macromolecule*, **27**, 2615 (1994).
24. J. Xu, S. Srinivas, H. Marand, and P. Agrawal, *Macromolecules*, **31**, 8230 (1998).
25. S. Z. D. Cheng, J. J. Janimak, A. Zhang, and H. N. Cheng, *Macromolecules*, **23**, 298 (1990).
26. J. J. Janimak, S. Z. D. Cheng, P. A. Giusti, and E. T. Hsieh, *Macromolecules*, **24**, 2253 (1991).
27. E. J. Clark and J. D. Hoffman, *Macromolecules*, **17**, 878 (1984).
28. Celli, A. Fichera, C. Marega, A. Marigo, G. Paganetto, and R. Zannetti, *Eur. Polym. J.*, **29**, 1037 (1993).
29. M. Takayanagi and T. Yamashita, *J. Polym. Sci.*, **22**, 552 (1956).
30. M. Yasuniwa, S. Tsubakihara, K. Iura, Y. Ono, Y. Dan, and K. Takahashi, *Polymer*, **47**, 7554 (2006).
31. T. Hirose, T. Takita, K. Nakamura, S. Umemoto, and N. Okui, *Polym. Prepr. Jpn.*, **56**, 668 (2007).
32. S. Umemoto and N. Okui, *Polymer*, **43**, 1423 (2002).
33. N. Okui, S. Umemoto, R. Kawano, and A. Mamun, *Lect. Notes Phys.*, **714**, 391 (2007).
34. J. D. Hoffman and J. J. Weeks, *J. Res. Natl. Bur. Stand.*, **66A**, 13

(1962).

35. J. L. Lauritzen and J. D. Hoffman, *J. Res. Natl. Bur. Stand.*, **64A**, 73 (1960).

36. P. Juhasz, J. Varga, K. Belina, and G. Belina, *J. Macromol. Sci.*, **B41**, 1173 (2002).

37. J. Varga, *Makromol. Chem.*, **112**, 161 (1983).

38. G. E. W. Schulze and H. P. Wilbert, *Colloid Polym. Sci.*, **267**, 108 (1989).

39. A. J. Lovinger and D. J. Freed, *Macromolecules*, **13**, 989 (1980).

40. K. Kawashima, R. Kawano, T. Miyagi, S. Umemoto, and N. Okui, *J. Macromol. Sci.*, **B42**, 889 (2003).

41. G. Guerra, V. Petraccone, P. Corradini, C. De Rosa, R. Napolitano, B. Pirozzi, and G. Giunchi, *J. Polym. Sci., Polym. Phys. Ed.*, **22**, 1029

42. Y. S. Yadav and P. C. Jain, *Polymer*, **27**, 721 (1986).

43. R. Napolitano, B. Pirozzi, and V. Varriale, *J. Polym. Sci., Part B: Polym. Phys.*, **28**, 139 (1990).

44. M. Naiki, T. Kikkawa, Y. Endo, K. Nozaki, T. Yamamoto, and T. Hara, *Polymer*, **42**, 5471 (2001).

45. T. Miyoshi, W. Hu, H. Hasegawa, L. Youngjin, A. Kaito, and K. Nakayama, *Polym. Prepr. Jpn.*, **56**, 679 (2007).

46. C. De Rosa, G. Guerra, R. Napolitano, V. Petraccone, and B. Pirozzi, *J. Thermal Anal.*, **30**, 1331 (1985).

47. G. C. Rutledge and U. W. Suter, *Macromolecules*, **25**, 1546 (1992).

48. W. Xu, D. C. Martin, and E. M. Arruda, *Polymer*, **46**, 455 (2005).